PERGAMON

International Journal of Solids and Structures 39 (2002) 725–739

INTERNATIONAL JOURNAL OF SOLIDS and STRUCTURES

www.elsevier.com/locate/ijsolstr

Vibration analysis of spinning cylindrical shells by finite element method

Dan Guo [a,*], Zhaochang Zheng [b,1], Fulei Chu [a]

[a] *State Key Laboratory of Tribology, Department of Precision Instruments, Tsinghua University, Beijing 100084, People's Republic of China*

[b] *Department of Engineering Mechanics, Tsinghua University, Beijing 100084, People's Republic of China*

Received 18 February 2000

Abstract

The vibration of spinning cylindrical shells are analyzed by using nine-node super-parametric finite element with shear and axial deformation and rotatory inertia. The non-linear plant-shell theory for large deflection is used to handle the cylindrical shell before it reaches equilibrium state by centrifugal force. Hamilton principle is used to present the motion equation of finite element form. The effects of Coriolis acceleration, centrifugal force, initial tension and geometric non-linearity due to large deformation are considered in this model. The effect of geometric non-linearity of large deformation on the frequency of spinning cylindrical shells, the effect of boundary conditions on the frequency parameter of spinning cylindrical shells and the effect of rotation speed on the different modes of spinning cylindrical shells have been investigated in detail.

Keywords: Spinning cylindrical shells; Forward wave; Backward wave; Geometric non-linearity; Finite element method

1. Introduction

Spinning cylindrical shells are used in various industrial equipments such as gas turbines, locomotive engines, high-speed centrifugal separators and rotor systems. Because the study on the vibration of spinning cylindrical shells is essential to understanding of rotating structures, many researchers have been interested in this topic.

The first recorded work on rotating cylindrical shells was by Bryan (1890), in which the phenomenon of traveling modes was first discovered. Later work on rotating shells included the study of the Coriolis effect on the free vibration by Taranto and Lesson (1964), by Srinivasan and Lauterbach (1971) for infinite long rotating shells, and by Zohar and Aboudi (1973) for finite length rotating shells. Other work included the study of long rotating cylinders subjected to pre-stress by Padovan (1973), the study of the effect of initial tensions by Saito and Endo (1986), the study of rotating conical shell by Lam and Li (1997, 1999) and

* Corresponding author. Tel.: +8610-62783968; fax: +8610-62781379.
E-mail address: guod@ntl.pim.tsinghua.edu.cn (D. Guo).
[1] Tel.: +8610-62785405.

0020-7683/02/$ - see front matter
PII: S0020-7683(01)00031-2

Sivadas (1995), the study of effects of boundary conditions on the frequency characteristics by Li and Lam (1998), and the study of rotating composite cylinders by Padovan (1975), Rand and Stavsky (1991), Lam and Loy (1994, 1995a,b), and Lee and Kim (1998). Endo et al. (1984) studied the flexural vibration of a thin rotating cylindrical ring especially from the experimental point of view, and compared the experimental results with theoretical results.

In the above studies on rotating cylindrical shells, much of the work was restricted to simply supported boundary condition. A few studies involving other boundary conditions were Saito and Endo (1986), Rand and Stavsky (1991), Penzes and Kraus (1972) and Lam and Li (1999). The studies involved clamped–clamped (C–C) boundary condition, simply supported–clamped (S–C) condition and simply supported–simply supported (S–S) condition. Only Rand and Stavsky (1991) studied the clamped–free condition, but the effect of this boundary condition on the frequency characteristics of the rotating cylindrical shell was not considered. None of them compared the frequency characteristics of rotating cylinders under the free–free (F–F) boundary condition with that under other boundary conditions.

Most of the researchers used analytical method to study the vibration of rotating cylindrical shell. It is difficult to solve the dynamic equation in general form by analytical method. For cylindrical shells and circular plates the series form solutions can be found, but these are not convergent in general. For a cylindrical shell the analytical solutions are valid only for some particular boundary conditions (Chen et al., 1993). Some researchers (Saito and Endo, 1986) had to hypothesize the shape function of vibration, and some assumptions had to be adopted, for example, pure bending assumption, small deformation assumption and so on (Endo et al., 1984). Lam and Li (1999) used trial function to solve the analytical equation, but sometimes the trial function can only satisfy the geometric boundary conditions and the improvement of numerical accuracy is difficult. So other methods had to be found to solve this problem (Li and Lam, 1998). However, the numerical solutions can be obtained by finite element methods in the general case and without imposing any restriction on the mode shapes. Of the document we have read, only a few studies were on the vibration of rotating cylindrical shells by finite element method. These include Padovan (1975), Chen et al. (1993), Sivadas and Ganesan (1994) and Sivadas (1995). Padovan (1975) developed a quasi-analytical finite element to study the traveling wave vibrations of rotating shell. The effects of Coriolis forces and centrifugal forces had been considered, but the influence of initial hoop tension due to the centrifugal force had been overlooked in the analysis of the fundamental equation. Sivadas (1995) studied the vibration of pre-stressed rotating thick circular shell by finite element method, and the shear deformation and rotatory inertia had been considered in his model. Because the axisymmetric finite element was used, some vibrational mode such as torsion mode and beam bending mode cannot be obtained. Chen et al. (1993) used the finite element method to solve the rotating cylindrical shell with high speed, and he considered the large deformation. In four papers mentioned above, no attempt was made to study the effect of non-linearity of large deformation due to centrifugal force on the frequency characteristics of rotating circular shells, and the effect of rotation on the displacement distribution of different mode has not been studied too.

As we know, the initial deformation due to centrifugal force is different under the different boundary conditions. For example, the initial deformation of rotating cylindrical shell under the clamped–free boundary condition is different from that under F–F boundary condition. Some researchers (Sivadas, 1995) concluded that the boundary conditions do not have any effect on the frequency parameter. But others concluded that the boundary conditions have effects on the frequency characteristics of rotating cylinders (Lam and Li, 1999). The contradictory conclusions prompted the present authors to investigate the vibration of spinning cylinders under different boundary conditions. A nine-node superparametric finite element is used. This paper has deduced the finite element form of spinning cylindrical shells. The non-linear plant-shell theory for large deflection is used to handle the cylindrical shell before it reaches the equilibrium state by centrifugal force, and then a linear approximation is employed. Not only the effect of Coriolis acceleration, centrifugal force and initial tension, but also the non-linearity due to large deformation is

considered in this model. The frequency characteristics of spinning cylinders with, respectively, the clamped–free boundary condition and F–F boundary condition are studied. The effects of non-linearity of large deformation on the normalized frequency of spinning cylindrical shells and the effects of rotation on different modes are studied. To examine the accuracy of the present analysis, comparisons are made against the results in the open literature for non-rotating and rotating cylindrical shells.

2. Theoretical formulation

The nine-node curvilinear finite element method is used in this paper (Fig. 1). The following assumptions are made:

- 'Normal line' to the middle surface remain straight after deformation.
- The stress component normal to the shell mid-surface is constrained to be zero.

Each node point has five degrees of freedom: u, v and w are three displacement components; α and β are two rotational angles in $\overline{V}_1$ and $\overline{V}_2$ directions. The detailed form of element description and derivation of the element stiffness matrix are available in the literature (Hinton and Owen, 1984). Only a brief introduction of finite element formulation for free vibration analysis is presented in the following.

The coordinates of a point within the element are obtained by applying the element shape functions to the nodal coordinates,

$$\begin{Bmatrix} x \\ y \\ z \end{Bmatrix} = \sum_{k=1}^{n} N_k \begin{Bmatrix} x_k \\ y_k \\ z_k \end{Bmatrix}_{\text{midsurface}} + \sum_{k=1}^{n} N_k \frac{h_k}{2} \varsigma \overline{V}_{3k} \tag{1}$$

where n is the number of node per element; $N_k = N_k(\xi, \eta)$ $(k = 1, n)$ are the element shape functions corresponding to the surface $\varsigma =$ constant; h_k is the shell thickness at node k; ξ, η, ς are the curvilinear coordinates of the point.

The element displacements can be expressed by

$$\begin{Bmatrix} u \\ v \\ w \end{Bmatrix} = \sum_{k=1}^{n} N_k \begin{Bmatrix} u_k \\ v_k \\ w_k \end{Bmatrix}_{\text{midsurface}} + \sum_{k=1}^{n} N_k \varsigma \frac{h_k}{2} \left[\overline{V}_{1k} - \overline{V}_{2k} \right] \begin{bmatrix} \alpha_k \\ \beta_k \end{bmatrix} \tag{2}$$

The expression of Eq. (2) can be simply written as

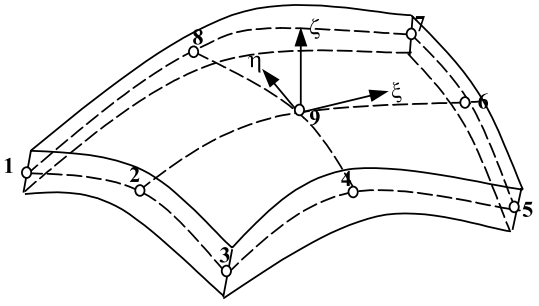

Fig. 1. Nine-node curvilinear finite element.

$$\overline{\delta} = \begin{Bmatrix} u \\ v \\ w \end{Bmatrix} = N\overline{a} \tag{3}$$

where

$$\overline{a} = \begin{Bmatrix} a_1 \\ a_2 \\ \vdots \\ a_9 \end{Bmatrix}, \quad a_i = \begin{Bmatrix} u_i \\ v_i \\ w_i \\ \alpha_i \\ \beta_i \end{Bmatrix} \quad (i = 1, 2, \ldots, 9) \tag{4}$$

N is the shape function matrix of the nine-node superparametric shell element $N = \left[\overline{N_1} \ \cdots \ \overline{N_k} \ \cdots \ \overline{N_9}\right]$, where

$$\overline{N_k} = \begin{bmatrix} N_k & 0 & 0 & N_k\varsigma\frac{h_k}{2}\overline{V}^x_{1k} & -N_k\varsigma\frac{h_k}{2}\overline{V}^x_{2k} \\ 0 & N_k & 0 & N_k\varsigma\frac{h_k}{2}\overline{V}^y_{1k} & -N_k\varsigma\frac{h_k}{2}\overline{V}^y_{2k} \\ 0 & 0 & N_k & N_k\varsigma\frac{h_k}{2}\overline{V}^z_{1k} & -N_k\varsigma\frac{h_k}{2}\overline{V}^z_{2k} \end{bmatrix} \quad (k = 1, 9) \tag{5}$$

According to the perturbation theory, we assume that the cylindrical shell's vibration is small around the equilibrium position. The non-linear plant-shell theory for large deflection is used to handle the cylindrical shell before it reaches the equilibrium state by centrifugal forces. The strain–displacement relation in local co-coordinate x, y, z is

$$\overline{\varepsilon} = \begin{Bmatrix} \varepsilon_x \\ \varepsilon_y \\ \gamma_{xy} \\ \gamma_{xz} \\ \gamma_{yz} \end{Bmatrix} = \begin{Bmatrix} \frac{\partial u}{\partial x} \\ \frac{\partial v}{\partial y} \\ \frac{\partial u}{\partial y} + \frac{\partial v}{\partial x} \\ \frac{\partial u}{\partial z} + \frac{\partial w}{\partial x} \\ \frac{\partial v}{\partial z} + \frac{\partial w}{\partial y} \end{Bmatrix} + \begin{Bmatrix} \frac{1}{2}\left[\left(\frac{\partial u}{\partial x}\right)^2 + \left(\frac{\partial v}{\partial x}\right)^2 + \left(\frac{\partial w}{\partial x}\right)^2\right] \\ \frac{1}{2}\left[\left(\frac{\partial u}{\partial y}\right)^2 + \left(\frac{\partial v}{\partial y}\right)^2 + \left(\frac{\partial w}{\partial y}\right)^2\right] \\ \frac{\partial u}{\partial x}\frac{\partial u}{\partial y} + \frac{\partial v}{\partial x}\frac{\partial v}{\partial y} + \frac{\partial w}{\partial x}\frac{\partial w}{\partial y} \\ \frac{\partial u}{\partial y}\frac{\partial u}{\partial z} + \frac{\partial v}{\partial y}\frac{\partial v}{\partial z} \\ \frac{\partial u}{\partial z}\frac{\partial u}{\partial x} + \frac{\partial v}{\partial z}\frac{\partial v}{\partial x} \end{Bmatrix} = \overline{\varepsilon}_l + \overline{\varepsilon}_n \tag{6}$$

where the non-linear strain component is

$$\overline{\varepsilon}_n = \tfrac{1}{2}SR \tag{7}$$

and

$$S = \begin{bmatrix} H_1^{\mathrm{T}} & 0 & 0 \\ 0 & H_2^{\mathrm{T}} & 0 \\ H_2^{\mathrm{T}} & H_1^{\mathrm{T}} & 0 \\ 0 & H_3^{\mathrm{T}} & H_2^{\mathrm{T}} \\ H_3^{\mathrm{T}} & 0 & H_1^{\mathrm{T}} \end{bmatrix} \tag{8}$$

$$R = \begin{bmatrix} H_1 \\ H_2 \\ H_3 \end{bmatrix} = T\overline{a} \tag{9}$$

where

$$H_1 = \begin{bmatrix} \frac{\partial u}{\partial x} \\ \frac{\partial v}{\partial x} \\ \frac{\partial w}{\partial x} \end{bmatrix}, \qquad H_2 = \begin{bmatrix} \frac{\partial u}{\partial y} \\ \frac{\partial v}{\partial y} \\ \frac{\partial w}{\partial y} \end{bmatrix}, \qquad H_3 = \begin{bmatrix} \frac{\partial u}{\partial z} \\ \frac{\partial v}{\partial z} \\ \frac{\partial w}{\partial z} \end{bmatrix} \tag{10}$$

$$T = [\, T_1 \;\; T_2 \;\; \cdots \;\; T_4 \,], \qquad T_i = \begin{bmatrix} \frac{\partial N_i}{\partial x} I \\ \frac{\partial N_i}{\partial y} I \\ \frac{\partial N_i}{\partial z} I \end{bmatrix} \tag{11}$$

Differential representation of Eq. (7) is:

$$\mathrm{d}\overline{\varepsilon}_n = \tfrac{1}{2}\mathrm{d}S R + \tfrac{1}{2} S\,\mathrm{d}R = ST\,\mathrm{d}\overline{a} = B_n\,\mathrm{d}\overline{a} \tag{12}$$

The matrix of strain–displacement relationship is taken in the form

$$B = B_l + B_n \tag{13}$$

The elements of the matrix B are not constant for non-linear shells with large deformation.

From Eqs. (12), (13) and (6), we can obtain

$$B_n = ST \tag{14}$$

The tangential stiffness matrix in geometric non-linear problem has the expression

$$K\,\mathrm{d}\overline{a} = [K_0 + K_\sigma]\,\mathrm{d}\overline{a} = \mathrm{d}P = \int_V B^{\mathrm{T}}\,\mathrm{d}\overline{\sigma}\,\mathrm{d}V + \int_V \mathrm{d}B^{\mathrm{T}}\overline{\sigma}\,\mathrm{d}V \tag{15}$$

because

$$\overline{\sigma} = D\overline{\varepsilon} = DB\overline{a} \tag{16}$$

We have

$$K_0 = \int_V B^{\mathrm{T}} DB\,\mathrm{d}V \tag{17}$$

$$K_\sigma\,\mathrm{d}\overline{a} = \int_V \mathrm{d}B^{\mathrm{T}}\overline{\sigma}\,\mathrm{d}V = \int_V \mathrm{d}B_n^{\mathrm{T}}\overline{\sigma}\,\mathrm{d}V \tag{18}$$

Substituting Eq. (14) into Eq. (18) gives

$$K_\sigma\,\mathrm{d}\overline{a} = \int_V T^{\mathrm{T}}\mathrm{d}S^{\mathrm{T}}\overline{\sigma}\,\mathrm{d}V \tag{19}$$

From Eqs. (8) and (9), we have

$$\mathrm{d}S^{\mathrm{T}}\overline{\sigma} = [\sigma]T\,\mathrm{d}\overline{a} \tag{20}$$

where

$$\sigma = \begin{bmatrix} \sigma_{xx} I & \tau_{xy} I & \tau_{xz} I \\ \tau_{yx} I & \sigma_{yy} I & \tau_{yz} I \\ \tau_{zx} I & \tau_{zy} I & \sigma_{zz} I \end{bmatrix} \tag{21}$$

Substituting Eq. (20) into Eq. (19), we can obtain

$$K_\sigma = \int_V T^{\mathrm{T}}[\sigma]T\,\mathrm{d}V \tag{22}$$

We assume that the cylindrical shell's vibration is small around the new equilibrium position. The shell is assumed to be rotating at constant angular velocity $\overline{\Omega}$ about its center axis which get across a reference point O. A location vector $\overline{r}_0$ can be defined from point Q of the shell to the fixed reference point O, the corresponding elasticity deformation vector is $\overline{\delta}(r_0, t)$, the velocity vector of deformation is $\dot{\overline{\delta}}$, and the total displacement of the point Q is

$$\overline{r} = \overline{r}_0 + \overline{\delta} \tag{23}$$

The corresponding velocity is

$$\overline{v} = \overline{\Omega} \times \overline{r} + \dot{\overline{\delta}} \tag{24}$$

where

$$\overline{r}_0 = \begin{Bmatrix} r_{0x} \\ r_{0y} \\ r_{0z} \end{Bmatrix}, \qquad \overline{\delta} = \begin{Bmatrix} u \\ v \\ w \end{Bmatrix}, \qquad \overline{\Omega} = \begin{Bmatrix} \Omega_x \\ \Omega_y \\ \Omega_z \end{Bmatrix}, \tag{25}$$

Ω_x, Ω_y and Ω_z are the components of $\overline{\Omega}$ in global coordinate x, y and z respectively.

The kinetic energy of this point is

$$\Delta T = \tfrac{1}{2}\Delta m \cdot (\overline{\Omega} \times \overline{r}) \times (\overline{\Omega} \times \overline{r}) + \Delta m \cdot (\overline{\Omega} \times \overline{r}) \cdot \dot{\overline{\delta}} + \tfrac{1}{2}\Delta m \dot{\overline{\delta}} \cdot \dot{\overline{\delta}} \tag{26}$$

For the whole element the kinetic energy can be written as the following expression

$$T = \frac{1}{2}\int_V \left(\dot{\overline{\delta}}^{\mathrm{T}}\dot{\overline{\delta}} + 2\dot{\overline{\delta}}^{\mathrm{T}}\underline{\Omega}\overline{\delta} + \overline{\delta}^{\mathrm{T}}\underline{\Omega}^{\mathrm{T}}\underline{\Omega}\overline{\delta} + 2\overline{r}_0^{\mathrm{T}}\underline{\Omega}^{\mathrm{T}}\dot{\overline{\delta}} + 2\overline{r}_0^{\mathrm{T}}\underline{\Omega}^{\mathrm{T}}\underline{\Omega}\overline{\delta}\right)\mathrm{d}m \tag{27}$$

where

$$\underline{\Omega} = \begin{bmatrix} 0 & -\Omega_z & \Omega_y \\ \Omega_z & 0 & -\Omega_x \\ -\Omega_y & \Omega_x & 0 \end{bmatrix} \tag{28}$$

By substituting Eq. (3) into Eq. (27), we obtain

$$T = \tfrac{1}{2}\dot{\overline{a}}^{\mathrm{T}}M\dot{\overline{a}} + \tfrac{1}{2}\dot{\overline{a}}G\overline{a} + \tfrac{1}{2}\overline{a}^{\mathrm{T}}K_c\overline{a} + \overline{a}^{\mathrm{T}}I + \dot{\overline{a}}^{\mathrm{T}}A + \dot{\overline{a}}^{\mathrm{T}}J\overline{a} \tag{29}$$

where

$$M = \int_V N^{\mathrm{T}}N\,\mathrm{d}m, \qquad G = 2\int_V N^{\mathrm{T}}\underline{\Omega}N\,\mathrm{d}m, \qquad K_c = \int_V N^{\mathrm{T}}\underline{\Omega}^{\mathrm{T}}\underline{\Omega}N\,\mathrm{d}m \tag{30}$$

K_c is the matrix due to the rotation of a particular element and G is the matrix due to Coriolis acceleration. The expressions of I, A and J will not be written in this paper because they do not appear in the motion equation.

The elemental potential energy is

$$V = \tfrac{1}{2}\overline{a}^{\mathrm{T}}K\overline{a} \tag{31}$$

From Eqs. (29) and (31), using Halmilton's principle, the perturbation motion equation of the shell about its equilibrium position is obtained

$$M\ddot{\overline{a}} + G\dot{\overline{a}} + (K - K_c)\overline{a} = 0 \tag{32}$$

where $K = [K_0 + K_\sigma]$ can be obtained from Eqs. (17) and (22).

3. Results and discussion

In this paper, the R, L and h are respectively the mean radius, length and thickness of the cylindrical shell. E, μ and ρ are respectively the elastic modula, Poisson's ratio and mass density of material, and n and m are respectively half the number of the circumferential node and the number of the longitudinal node.

In order to verify the program and the present method, two comparisons with the results in the open literature are made in Tables 1 and 2.

The first, as shown in Table 1, involves the free vibration of a non-rotating cylindrical shell with clamped–free boundary condition. The dimension and material properties of the cylindrical shell is same as that of reference (Chung, 1981). A comparison between the present results and the results of Chung (1981) is made in Table 1. For a pure numerical approach, the scheme of the discretization meshing has influence on calculation results. From Table 1, it can be seen that for a given m and n, if the circumferential element number is greater than three times n and the longitudinal element number is greater than two times m, the percent error between the present result and the analytical result of Chung (1981) is less than 5%.

The second, as shown in Table 2, involves the free vibration of a long spinning cylindrical shell and makes a comparison between the present result and the result from the equation of Endo et al. (1984), it can be observed that very good agreement is achieved.

The shells discussed in the following are thin cylindrical shells rotating about the center axis (Fig. 2). The geometric properties and material properties are:

Table 1
Comparison of natural frequency for a non-rotating cylindrical shell with clamped–free boundary condition

n	m	Chung[a] (Hz)	Present (12×6)[b] (Hz)	Present (16×8) (Hz)	Present (20×3) (Hz)	Present (20×10) (Hz)
1	1	855.10	855.83(0.08%)[c]	855.83(0.08%)	855.77(0.08%)	855.83(0.08%)
2	1	403.72	405.39(0.40%)	404.60(0.20%)	404.35(1.6%)	404.34(0.15%)
3	1	223.34	227.15(1.7%)	224.73(0.6%)	224.14(0.36%)	223.95(0.27%)
4	1	171.77	179.29(4.4%)	173.80(1.2%)	172.47(0.41%)	172.09(0.19%)
5	1	199.16	218.37(9.6%)	204.13(2.5%)	200.37(0.61%)	199.93(0.39%)
6	1	268.86	319.01(19%)	284.06(5.4%)	273.66(1.8%)	273.20(1.6%)
7	1	361.92	503.79(39%)	402.21(11%)	376.55(4.0%)	376.00(3.9%)
8	1	472.54	824.30(74%)	565.51(20%)	508.14(7.5%)	507.43(7.4%)
1	2	2318.98	2320.99(0.09%)	2320.79(0.09%)	–	2320.63(0.07%)
2	2	1437.11	1436.11(−0.07%)	1440.01(0.2%)	1446.94(0.68%)	1439.11(1.4%)
3	2	928.28	920.82(−0.8%)	934.60(0.7%)	938.23(1.1%)	931.82(0.4%)
4	2	644.48	635.01(−1.5%)	656.49(1.9%)	655.51(1.7%)	650.51(0.94%)
5	2	494.69	490.30(−0.9%)	514.28(4.0%)	507.25(2.5%)	503.69(1.8%)
6	2	442.00	638.66(44%)	473.10(7.0%)	457.22(3.4%)	455.09(3%)
7	2	464.59	715.07(54%)	518.47(12%)	487.20(5%)	486.24(4.7%)
8	2	539.45	–	618.16(15%)	580.53(7.6%)	580.38(7.6%)
1	3	3076.05	3078.40(0.08%)	3078.84(0.08%)	–	–
2	3	2487.60	–	2493.12(0.2%)	–	2491.37(0.15%)
3	3	1834.82	–	1841.93(0.4%)	–	1842.31(0.41%)
4	3	1367.64	–	1377.10(0.7%)	1450.45(6%)	1380.86(1%)
5	3	1057.12	–	1072.73(1.5%)	1140.61(8%)	1078.27(2%)
6	3	864.82	1053.40(21.8%)	890.22(3%)	950.64(10%)	895.92(3.6%)
7	3	767.65	–	801.95(4.5%)	858.47(12%)	811.74(5.7%)
8	3	750.67	–	676.03(10%)	853.25(13.67%)	814.78(8.5%)

[a] The result of Chung (1981).
[b] The circumferential element number is 12 and the longitudinal element number is 6.
[c] The percent error between the present result and the result of Chung (1981) is 0.08%.

Table 2
Comparison of frequencies for a long spinning cylindrical shell ($m = 1$, $\mu = 0.3$, $E = 2.07 \times 10^{11}$ N/m^2, $\rho = 7.86 \times 10^3$ kg/m^3, $h/R = 0.002$)

Ω (rev.p.s)	n	Endo et al.[a]		Present result	
		f_b (Hz)	f_f (Hz)	f_b (Hz)	f_f (Hz)
0.5	2	6.0974	6.8974	6.0545	6.9314
	3	4.6508	5.2508	4.5905	5.2521
	4	7.5014	7.9719	7.4396	7.9643
	5	12.5790	12.9641	12.5251	12.9634
1.0	2	5.7799	7.3799	5.7142	7.4675
	3	4.7694	5.9694	4.7194	6.0421
	4	7.8480	8.7891	7.7829	8.8791
	5	12.9975	13.7667	13.0234	13.8973

[a] From the equation of Endo et al. (1984)

$$\omega_f = \left(\frac{2n}{n^2+1} \frac{\Omega}{\omega_0} - \left(1 + \frac{n^2(n^2-1)^2}{(n^2+1)^2} \frac{\Omega}{\omega_0} \right)^{1/2} \right) \omega_0$$

$$\omega_b = \left(\frac{2n}{n^2+1} \frac{\Omega}{\omega_0} + \left(1 + \frac{n^2(n^2-1)^2}{(n^2+1)^2} \frac{\Omega}{\omega_0} \right)^{1/2} \right) \omega_0$$

where ω_f and ω_b are respectively the forward wave frequency and backward wave frequency of the shell spinning at a speed Ω, ω_0 is the frequency of the shell when $\Omega = 0$.

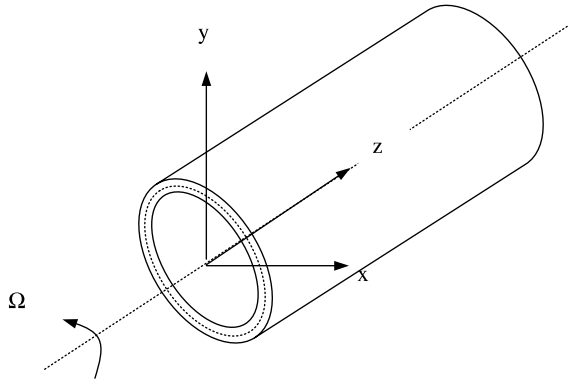

Fig. 2. Geometry of a thin spinning cylindrical shell.

$$L = 0.5 \text{ m}, \qquad R = 0.5 \text{ m}, \qquad h = 0.02 \text{ m}$$
$$E = 2.07 \times 10^{11} \text{ N/m}^2, \qquad \upsilon = 0.3, \qquad \rho = 7.86 \times 10^3 \text{ kg/m}^3$$

The boundary conditions are F–F boundary condition and free–clamped (F–C) boundary condition. The scheme of discretization mesh adopted in this paper is that 30 elements were divided on circumference and five elements on length. So the whole finite element number is 30 times 5.

The first study of this paper is to investigate the effect of non-linearity of large deformation on the frequency of the spinning cylindrical shells. From Eq. (13), it is observed that the matrix of strain–displacement relationship B is not constant for a large deformation non-linear shell, B consists of two parts, the matrix B_l, which does not change with the deformation of shells, and the matrix B_n, which

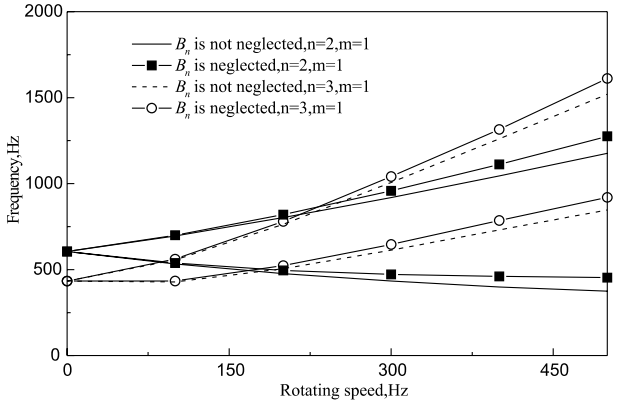

Fig. 3. Natural frequency at different modes of vibration as a function of the rotating speed for a F–C spinning cylindrical shell.

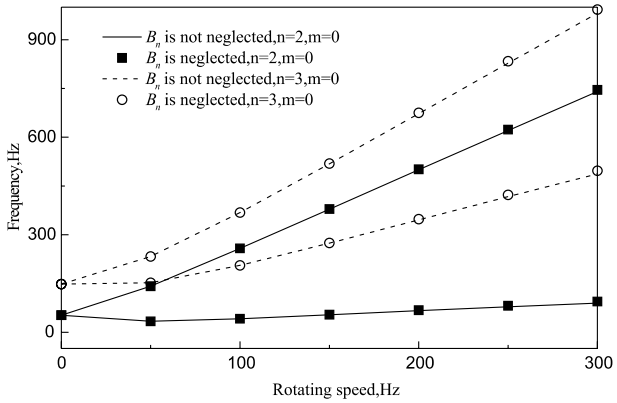

Fig. 4. Natural frequency at different modes of vibration as a function of the rotating speed for a F–F spinning cylindrical shell.

varies with the change of deformation. B_n is often omitted if the deflection of the shell is small. Figs. 3–6 illustrate the influence of B_n on the frequency of the spinning cylindrical shells with different rotating speeds and boundary conditions. Fig. 3 shows the variation of the natural frequency of a F–C cylindrical shell with the rotational speed for the B_n neglected and not neglected, and Fig. 4 shows that for F–F boundary condition. The trends of all curves are the same as in literatures (Saito and Endo, 1984; Sivadas, 1995; Li and Lam, 1998). For one rotating speed, the backward wave frequency and the forward wave frequency are present, and they increase monotonically with the rotational speed if $n > 2$. It is observed from Fig. 3 that there is very little difference between the natural frequencies for B_n neglected and that for B_n not neglected at low rotational speed. However, this difference increases when the rotational speed increases. The curves of frequency for B_n not neglected always lie below that for B_n neglected. But from Fig. 4, it is found that the B_n does not have any obvious influence on the frequencies at all rotational speed range. The variations of the frequency errors for the B_n neglected and not neglected with the rotational speed are shown in Fig. 5. The errors increase obviously with the rotating speed for F–C boundary condition, and the effects of B_n on the frequencies of forward wave and backward wave are different. The effect on backward wave frequency is larger than that on forward wave when spinning at high speed. But for F–F boundary condition, the errors have little change with the rotating speed, and the effects of B_n on the frequencies of

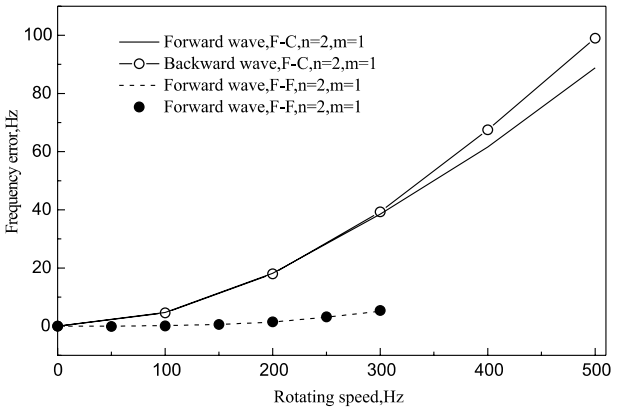

Fig. 5. Frequency error between the case of omitting B_n and not omitting B_n at different boundary conditions as a function of the rotating speed.

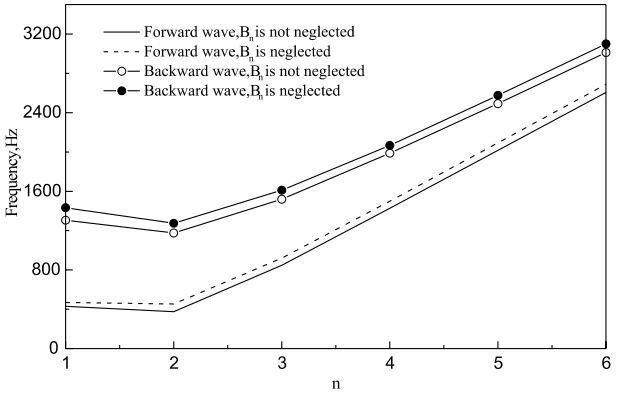

Fig. 6. Natural frequency as a function of circumferential wave number n for a F–C spinning cylindrical shell ($m = 1$).

forward wave and backward wave are not found different. It is known that for a spinning cylindrical shell there is different initial deformation due to centrifugal force for different boundary conditions. For F–F boundary condition, the initial displacement is almost homogeneous along the length of the cylindrical shell. But for F–C boundary condition, the initial displacement is not homogeneous. It results in the different effect of B_n on the frequency of the spinning cylindrical shell for different boundary conditions. Fig. 6 illustrates the effect of B_n on the frequencies of an F–C cylindrical shell spinning at $\Omega = 500$ Hz. It shows that the frequency of $n = 2$ are the lowest in every curve. The frequencies for B_n neglected are larger than those for B_n not neglected. From Eqs. (8)–(14), it can be obtained that B_n is a non-linear function of node's displacement. The iteration method must be adopted to obtain the values of B_n for one node's displacement. This process wastes most of the computer time. For example, using Pentium III 750 computer, it takes 11 min and 6 s to calculate the M, G and K_c of the F–C cylindrical shell spinning at $\Omega = 500$ Hz for B_n not neglected, while it only takes 1 min and 50 s for B_n neglected. From Figs. 3–6, it is concluded that the effect of B_n on the frequencies of an F–C cylindrical shell spinning at high speed cannot be neglected. But for F–F spinning cylindrical shells or F–C cylindrical shells with low rotating speed, the effects of B_n can be neglected, which is obtained by omitting the B_n term in Eq. (13), so the computer time can be reduced much.

The second study of this paper is to investigate the effect of boundary conditions on the frequency parameter of the spinning cylindrical shells. For ease of comparison and discussion, a normalized frequency $\omega^* = \omega/\omega_0$ and normalized rotating speed $\Omega^* = \Omega/\omega_0$ are used. The results are shown in Figs. 7–10. The relationship between the frequency of stationary cylindrical shells with different boundary conditions and the circumferential wave number n is shown in Fig. 7 for different longitudinal node number m. As shown in the figure, the F–C cylindrical shell has the higher frequency than F–F shell for the same m. Although the frequency of the cylindrical shell with the same m does not monotonically increase with the circumferential wave number n, for the same n, the frequency with larger m is higher than that for smaller one. When the cylindrical shell is spinning at $\Omega = 100$ Hz, the relationship between the frequency with different boundary conditions and the circumferential number n is shown in Fig. 8 for $m = 0$. From this figure, it is seen that the difference between the frequencies of F–F and F–C boundary conditions is large for the small circumferential wave number n, while it is relatively small for the large n. This conclusion is the same as that in the literature (Li and Lam, 1998), which studied the effects of S–C, C–C and S–S boundary conditions. Figs. 9 and 10 show the variation of the normalized frequency ω^* with normalized rotating speed Ω^* for F–F boundary condition and F–C boundary condition, respectively, and for $n = 2$, $m = 0$ and $n = 3$, $m = 0$. In

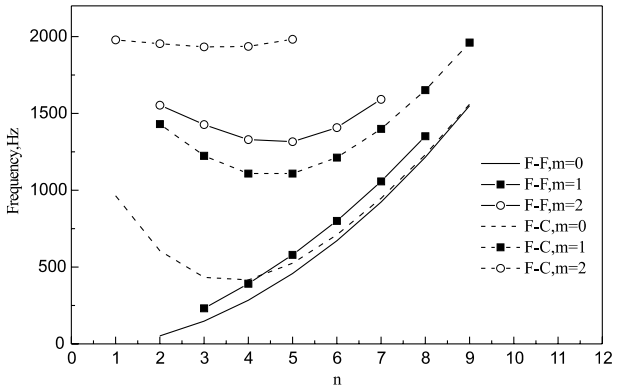

Fig. 7. The relationship between the frequency of cylindrical shells with different boundary conditions and the circumferential number n for different longitudinal wave number m at $\Omega = 0$.

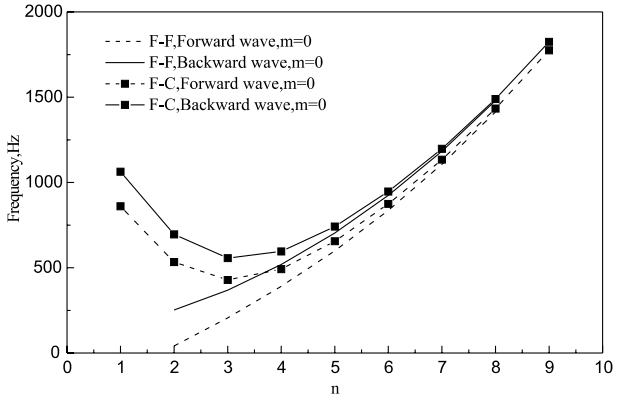

Fig. 8. The relationship between the frequency of the spinning cylindrical shell with different boundary conditions and the circumferential number n for $m = 0$, $\Omega = 100$ Hz.

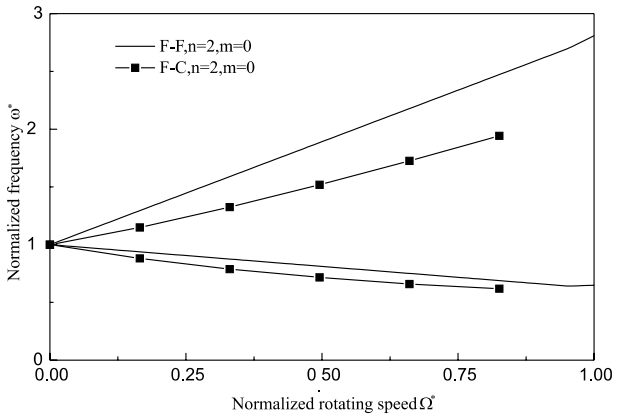

Fig. 9. The relationship between the normalized frequency of shells with different boundary conditions and the rotating speed for $n = 2$, $m = 0$.

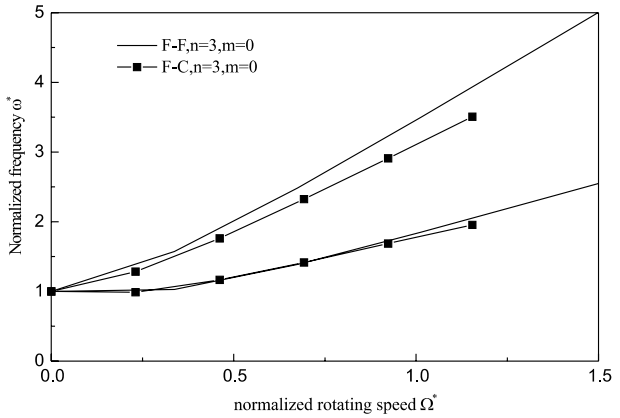

Fig. 10. The relationship between the normalized frequency of shells with different boundary conditions and the rotating speed for $n = 3$, $m = 0$.

both figures, the ω^* for two waves of F–C lies below that of F–F, and the difference between the backward wave frequency of F–F and that of F–C is larger than that for forward wave. It shows that the deviation between the ω^* of F–C shell and F–F shell for $n = 2$ is larger than that for $n = 3$ from Figs. 9 and 10.

The third study of this paper is to investigate the effect of the rotational speed on the mode of the F–F cylindrical shell. Three kinds of modes studied are shown in Fig. 11(a)–(c). The circumferential wave number of all three kinds of modes is 2, and the longitudinal node number is 0, 1 and 2, respectively. For ease of comparison and discussion, the mean percent ratio of displacement distribution corresponding to radial, tangential and longitudinal directions is defined as u_r^*, u_t^*, u_z^*, respectively, and

$$u_j^* = 100\sqrt{\frac{1}{k}\sum_{i=1}^{k} u_{ji}^2}\Bigg/\left(\sum_j \sqrt{\frac{1}{k}\sum_{i=1}^{k} u_{ji}^2}\right), \quad j = r, t, z \tag{33}$$

where k is the whole number of finite element nodes of the cylindrical shell. u_{ji} is the displacement of node i corresponding to j direction. Table 3 shows the mean percent ratio of displacement distribution of three

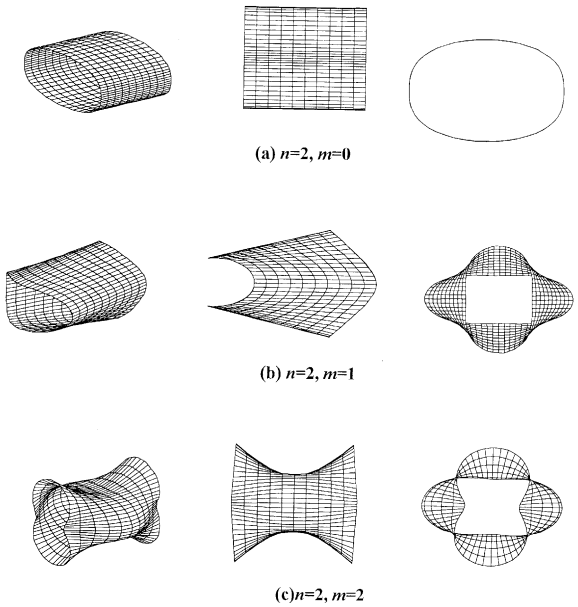

Fig. 11. Three kinds of modes of the F–F rotating cylindrical shell at $\Omega = 50$ Hz.

Table 3
The mean percent ratio of displacement distribution of three modes of a F–F thin cylindrical shell at $\Omega = 0$ Hz

Mode	u_r^*	u_t^*	u_z^*
$n = 2$, $m = 0$	67	34	0
$n = 2$, $m = 1$	44	22	34
$n = 2$, $m = 2$	88	9	3

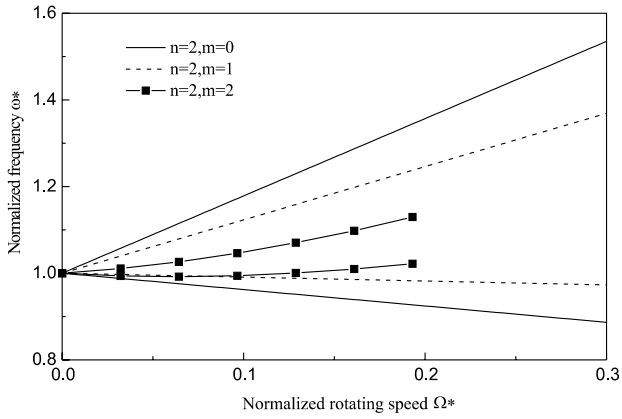

Fig. 12. The relationship between the normalized frequency and rotating speed for the F–F spinning cylindrical shell, and for different modes.

modes of a stationary thin cylindrical shell with F–F boundary condition. From Table 3, it is shown that the percent ratio of displacement for different modes is different. Fig. 12 shows the variation of the normalized frequency ω^* with normalized rotating speed Ω^* for F–F boundary condition, and for $n = 2$ and

$m = 0$, $n = 2$ and $m = 1$, $n = 2$ and $m = 2$, respectively. In the figure, the curves of ω^* for $n = 2$, $m = 0$ lie out of other modes' curves, followed similarly by the modes of $n = 2$, $m = 1$ and $n = 2$, $m = 2$. For studying the effects of rotating speed on the mean percent ratios of displacement distribution u_r^*, u_t^*, u_z^* for different modes, we calculate the u_r^*, u_t^*, u_z^* for mode $n = 2$, $m = 0$, $n = 2$, $m = 1$ and $n = 2$, $m = 2$ as the rotating speed varies from 0 to 300 Hz. The results show that the rotation has no obvious effect on the percent ratios of displacement distribution. So it is concluded that the rotation has different effect on the frequency of different modes, but has no obvious effect on the displacement distribution ratio of different modes.

4. Conclusions

Spinning cylindrical shells have been analyzed by using nine-node superparametric finite element method. The finite element form of the spinning cylindrical shell has been deduced. The shear and axial deformation and rotatory inertia have been considered in the finite element model. The effects of Coriolis acceleration, centrifugal force, initial tension and geometric non-linearity due to large deformation have been included in the physical model. The non-linear plant-shell theory for large deflection is used to handle the cylindrical shell before it reaches the equilibrium state by centrifugal force, and then a linear approximation is applied.

The effects of non-linearity of large deformation on the frequency of spinning cylindrical shells, the effects of boundary conditions on the frequency parameter of the spinning cylindrical shells and the effects of rotation speed on the different modes of a F–F cylindrical shell have been investigated. Based on the analysis, the conclusions can be drawn as follows:

1. The effect of non-linear strain–displacement relationship matrix B_n due to large deformation on the frequencies of F–C cylindrical shells rotating at high speed is obvious. But for F–F spinning cylindrical shells or F–C cylindrical shells with low rotating speed, this effect can be neglected.
2. The difference between the frequencies of F–F and F–C spinning cylindrical shells is large for the small circumferential wave number n, while it is relatively very small for the large n.
3. At one normalized rotating speed Ω^*, the normalized frequency ω^* for F–C cylindrical shells is smaller than that for F–F cylindrical shells. The difference between the normalized frequencies of F–F and F–C cylindrical shells for the backward wave is larger than that for the forward wave.
4. For the same n, the backward normalized frequency ω^* of F–F cylindrical shell is larger at a small m than at a big m, but the forward normalized frequency is reverse.
5. The rotation has different effect on the frequency of different modes, but has no obvious effect on the displacement distribution ratio of different modes.

Acknowledgements

This research is financially supported by National Key Basic Research Special Fund (no. G1998020316), and by National Natural Science Foundation of China (no. 19972029).

References

Bryan, G.H., 1890. On the beats in the vibration of revolving cylinder or bell. Proceedings of the Cambridge Philosophical Society 7 (1), 101–111.

Chen, Y., Zhao, H.B., Shen, Z.P., 1993. Vibrations of high speed rotating shells with calculations for cylindrical shells. J. Sound Vibr. 160 (1), 137–160.

Chung, H., 1981. Free vibration analysis of circular cylindrical shells. J. Sound Vibr. 74 (2), 331–350.

Endo, M., Hatamura, K., Sakata, M., Taniguch, O., 1984. Flexural vibration of a thin rotating ring. J. Sound Vibr. 92 (2), 261–272.
Hinton, E., Owen, D., 1984. Finite element software for plate and shells. Swansea, UK.
Lam, K.Y., Li, H., 1997. Vibration analysis of a rotating truncated circular conical shell. Int. J. Solids Struct. 34 (17), 2183–2196.
Lam, K.Y., Li, H., 1999. Influence of boundary conditions on the frequency characteristics of a rotating truncated circular conical shell. J. Sound Vibr. 223 (1), 171–195.
Lam, K.Y., Loy, C.T., 1995a. Analysis of rotating laminated cylindrical shells by different thin shell theories. J. Sound Vibr. 186 (1), 23–25.
Lam, K.Y., Loy, C.T., 1994. On vibrations of thin rotating laminated composite cylindrical shells. Compos. Engng. 4, 1153–1167.
Lam, K.Y., Loy, C.T., 1995b. Free vibrations of a rotating multi-layered cylindrical shell. Int. J. Sol. Struct. 32, 647–663.
Lee, Y.S., Kim, Y.W., 1998. Vibration analysis of rotating composite cylindrical shells with orthogonal stiffeners. Comp. Struct. 69, 271–281.
Li, H., Lam, K.Y., 1998. Frequency characteristics of a thin rotating cylindrical shell using the generalized differential quadrature method. Int. J. Mech. Sci. 40 (5), 443–459.
Padovan, J., 1973. Natural frequencies of rotating prestressed cylinders. J. Sound Vibr. 31 (2), 469–482.
Padovan, J., 1975. Travelling waves vibrations and buckling of rotating anisotropic shells of revolution by finite elements. Int. J. Solids Struct. 11 (12), 1367–1380.
Penzes, L.E., Kraus, H., 1972. Free vibration of prestresses cylindrical shells having arbitrary homogeneous boundary conditions. AIAA J. 10 (9), 1309–1314.
Rand, O., Stavsky, Y., 1991. Free vibrations of spinning composite cylindrical shells. Int. J. Solids Struct. 28 (7), 831–843.
Saito, T., Endo, M., 1986. Vibration of finite length rotating cylindrical shells. J. Sound Vibr. 107 (1), 17–28.
Srinivasan, A.V., Lauterbach, G.F., 1971. Travelling waves in rotating cylindrical shells. J. Engng. Indust. 93 (10), 1229–1232.
Sivadas, K.R., 1995. Vibration analysis of pre-stressed rotating thick circular conical shell. J. Sound Vibr. 186 (1), 99–109.
Sivadas, K.R., Ganesan, N., 1994. Effect of rotation on vibration of moderately thick circular cylindrical shells. J. Vibration Acoust. 116 (1), 198–202.
Taranto, D., Lesson, M., 1964. Coriolis acceleration effect on vibration of a rotating thin-walled circular cylinder. J. Appl. Mech. 31 (5), 700–710.
Zohar, A., Aboudi, J., 1973. The free vibrations of thin circular finite rotating cylinder. Int. J. Mech. Sci. 15 (2), 269–278.